Ceramics International 43 (2017) 4263–4271

Contents lists available at ScienceDirect

Ceramics International

journal homepage: www.elsevier.com/locate/ceramint

Rolling contact fatigue behavior of Ti/TiN coated ADI by cathodic arc deposition

Diego Alejandro Colombo[a,*], Juan Miguel Massone[a], María Dolores Echeverría[a], Adriana Beatriz Márquez[b]

[a] Instituto de Investigaciones en Ciencia y Tecnología de Materiales, UNMdP, CONICET, Facultad de Ingeniería, Av. J. B. Justo 4302, B7608FDQ Mar del Plata, Argentina

[b] Instituto de Física del Plasma, UBA, CONICET, Departamento de Física, FCEyN, Intendente Güiraldes 2160 Pabellón I PB Ciudad Universitaria, C1428EGA Ciudad de Buenos Aires, Argentina

ARTICLE INFO

Keywords:
Austempered ductile iron
Physical vapor deposition
Cathodic arc deposition
TiN
Ti interlayer
Rolling contact fatigue

ABSTRACT

This work studies the rolling contact fatigue (RCF) behavior of austempered ductile iron samples coated with Ti/TiN by cathodic arc deposition. The influence of the TiN layer thickness on the characteristics and RCF life of the coated samples is analyzed. RCF tests were performed in a flat washer type testing rig, using a thrust ball bearing as a counterpart. The maximum contact pressure was 1400 MPa. RCF tests results were analyzed using the two-parameter Weibull distribution. The rolling track of the tested samples was examined by using SEM and EDS.

The results show that the surface hardness, residual stresses and coating adhesion strength of the samples increase as TiN layer thickness increases while surface roughness, coating hardness and elastic modulus do not vary significantly with the TiN layer thickness. Regarding the RCF tests, two failure mechanisms were observed in the coated samples, coating delamination and substrate spalling. Coating delamination turned out to be the most predominant mechanism and occurred at fewer loading cycles than substrate spalling. The EDS analysis revealed that inside the delaminated areas the Ti interlayer remained adhered to the substrates in all the cases. Extended tests on delaminated samples show growing delamination until final failure by substrate spalling occurred. The Weibull analysis indicates that the RCF life of the coated samples seems to have a tendency to increase with the TiN layer thickness and, in the case of the thicker TiN layer, to exceed the life of uncoated ADI after the extended tests. However, due to the number of samples employed, the statistic analysis does not show significant differences in the RCF behavior of the uncoated and coated samples.

1. Introduction

Austempered ductile iron (ADI) is increasingly being used for the manufacturing of mechanical components subjected to rolling contact fatigue (RCF), such as gears and cams. RCF is a wear mechanism that appears in components subjected to rolling or rolling/sliding contacts. The cyclic loading of the contact bodies produces a near-surface alternating stress field, which leads to nucleation and growth of fatigue cracks and, eventually, to material removal. The material removal in coated surfaces can vary from coating delamination to substrate spalling. Several authors studied the RCF behavior of ADI with different nodule counts and austempering temperatures [1–5]. They figured out that ADI resistance to RCF increases as austempering temperature decreases, nodule count increases and surface roughness decreases. They also found that graphite nodules act as preferential sites for crack nucleation. Consequently, the use of surface treatments could offset the negative effect of the nodules.

The authors of the present work studied RCF behavior of ADI samples coated with TiN and CrN films by cathodic arc deposition (CAD), a physical vapor deposition (PVD) technique in which an electric arc is used to evaporate the cathode material [6,7]. It was found that the substrate surface finishing method, the coating material and its thickness affect the RCF resistance of the coated samples. Conventional grinding of the substrate surface improves the RCF life of the coated samples as compared to manual polishing. As coating thickness increased, within the analyzed range, the RCF life decreased. Samples with a coating thickness of 0.7 μm exhibited a higher RCF life than uncoated ADI with failures produced exclusively by substrate spalling. On the other hand, samples with coating thicknesses of 1.4 μm and 2.1 μm showed a lower RCF life than uncoated ADI with failures

* Corresponding author.
E-mail address: diegocolombo@fi.mdp.edu.ar (D.A. Colombo).

http://dx.doi.org/10.1016/j.ceramint.2016.12.068
Received 16 September 2016; Received in revised form 29 November 2016; Accepted 12 December 2016
Available online 13 December 2016

mainly produced by coating fracture and delamination. In addition, it was observed that graphite nodules present on the substrate surface act as preferential sites for coating delamination since there is a large mismatch in the mechanical and chemical properties between the coating material and the graphite of the nodules [6].

Ductile interlayers (e.g. Ti, Cr, Zr, Nb) have often been used as an alternative to improve the adhesion and wear properties of ceramic-based coated systems [8–12]. The introduction of two or more layers provides barriers to crack propagation [13]. Also, ductile interlayers might improve the load-bearing capacity as they provide a better stress distribution from the coating to the substrate [14]. In the case of TiN coatings, it is a common practice to incorporate a Ti interlayer. The main function of the Ti interlayer is to provide a template for the growth of TiN film due to the very good epitaxial relation between Ti and TiN [15]. Consequently, the introduction of a Ti interlayer could improve the RCF behavior of TiN coated ADI by reducing the properties mismatch between substrate and coating.

On this basis, the aim of this work is to study the RCF behavior ADI samples coated with Ti/TiN by CAD and to evaluate the influence of the TiN layer thickness on the characteristics and RCF life of the coated samples.

2. Experimental procedures

2.1. Substrate material and samples preparation

ADI samples used in this work were obtained from alloyed ductile iron castings. A detailed description of the casting process (melting, inoculation, nodulization and casting into sand moulds) was presented in detail elsewhere [7]. The chemical composition of the obtained material (wt%), analyzed by optical emission spectrometry, was as follows: C=3.35; Si=2.87; Mn=0.13; S=0.015; P=0.032; Mg=0.043; Cu=0.76; Ni=0.57 and Fe balanced. The nodule count of the samples was about 300 nod/mm^2, with an average nodule diameter of 20 μm. Based on chart comparisons (ASTM A247), nodularity exceeded 90% in all cases. The heat treatment consisted in an austenitising at 910 °C for 120 min, an austempering in a salt bath at 280 °C for 90 min, and a subsequent air cooling to room temperature. The average Brinell hardness obtained was 417 $HBW_{2.5/187.5}$. ADI samples were surface finished by conventional surface grinding, carried out on a horizontal-spindle surface grinder and under industrial-use cutting conditions. Three roughing passes and one finishing pass were conducted on each sample. The finishing pass aims to attain low surface roughness. A vitrified wheel with SiC abrasive grains, identified as IC36/46I/J5V9, was employed. A 5% aqueous solution of soluble oil was used as cooling fluid.

2.2. Coating process

Ti/TiN coatings were deposited by CAD in an experimental reactor and using sets of processing parameters specifically designed for ADI in order to avoid its microstructural degradation [16]. A detailed description of the CAD system was presented in a previous work [17]. The experiment was carried out with a discharge current of 100 A, establishing a cathode – anode voltage of 30 V. The base pressure of the system was below 10^{-3} Pa. The samples were mounted on a holder located at 200 mm in distance from the cathode front surface. The samples were thoroughly degreased, ultrasonically cleaned, rinsed with alcohol and dried with warm air. Inside the chamber, and prior to deposition, samples were exposed to an Ar glow discharge run with a current of 10 mA at a pressure of 100 Pa for 45 min.

During the coating process the substrates were kept at 300 °C and biased at −130 V respect to the anode. To deposit TiN films a nitrogen flow of ~ 40 sccm was introduced into the chamber with a working pressure in the range from 2×10^{-2} Pa to 4×10^{-2} Pa. Ti films with thicknesses in the range from 0.3 μm to 1.1 μm were deposited in order to characterize the Ti layer. For the Ti/TiN films, the deposition times were adjusted to obtain a nominal thickness of 0.3 μm for the Ti interlayer (5 min) and two different nominal thicknesses for the TiN layer, 0.7 μm (16 min) and 1.5 μm (35 min). The coated samples were identified as “ADI-Ti/TiN 0.7” and “ADI-Ti/TiN 1.5”, respectively.

Table 1
Deposition time and thickness of the different Ti layers.

Sample	Deposition time (min)	Layer thickness (μm)
ADI-Ti 0.3	5	0.29 ± 0.03
ADI-Ti 0.6	10	0.64 ± 0.05
ADI-Ti 1.1	20	1.10 ± 0.06

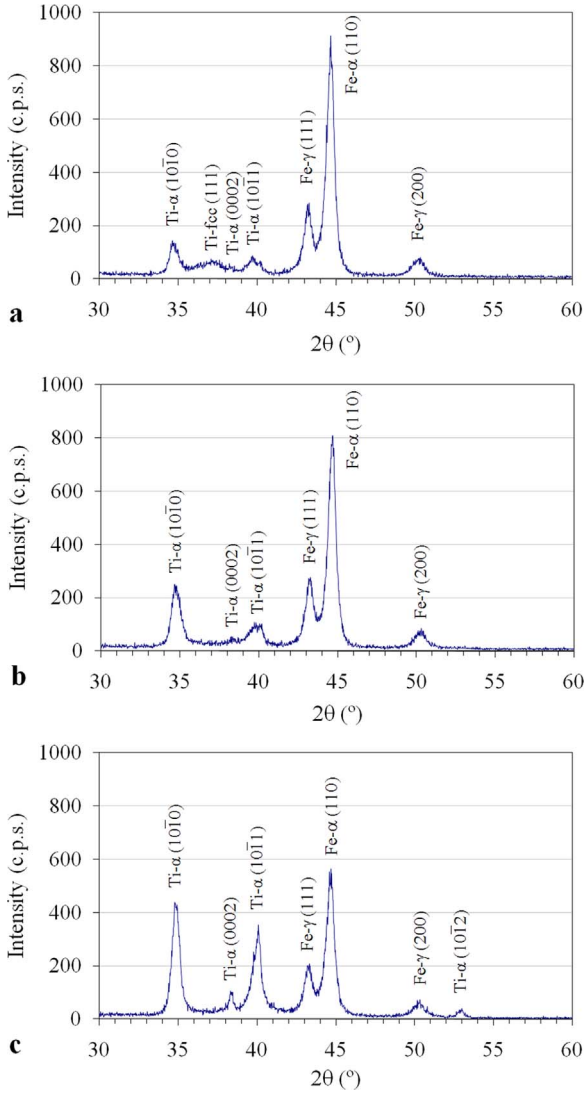

Fig. 1. DRX patterns of the Ti coated samples for the different layer thicknesses analyzed: (a) 0.3 μm, (b) 0.6 μm, (c) 1.1 μm.

2.3. Substrates and coatings characterization

Optical microscopy was utilized to identify the microstructure of ADI substrates before and after coating deposition. The metallographic characterization of the substrates after coating deposition was performed on cross sections and near the sample surface in order to identify possible degradation of the ADI structure. The conventional arithmetic average roughness of the uncoated and coated samples was analyzed using a stylus profiler. The surface hardness of the uncoated

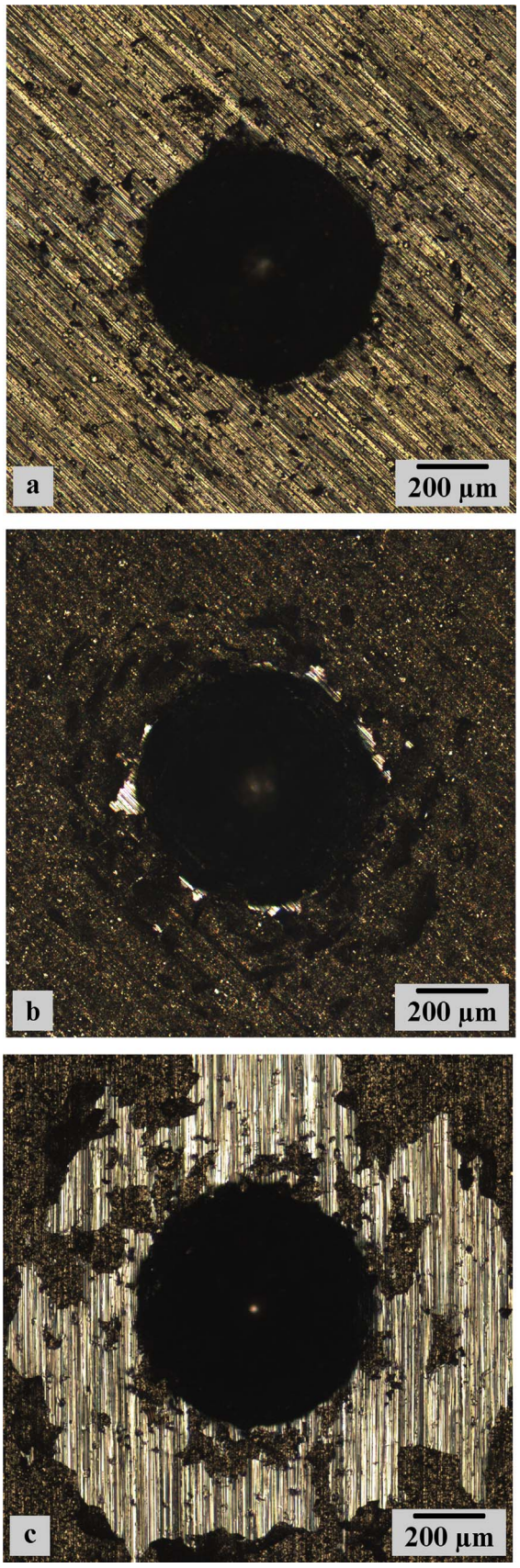

Fig. 2. Imprints on the Ti coated samples after Rockwell-C adhesion test for the different layer thicknesses analyzed: (a) 0.3 µm, (b) 0.6 µm, (c) 1.1 µm.

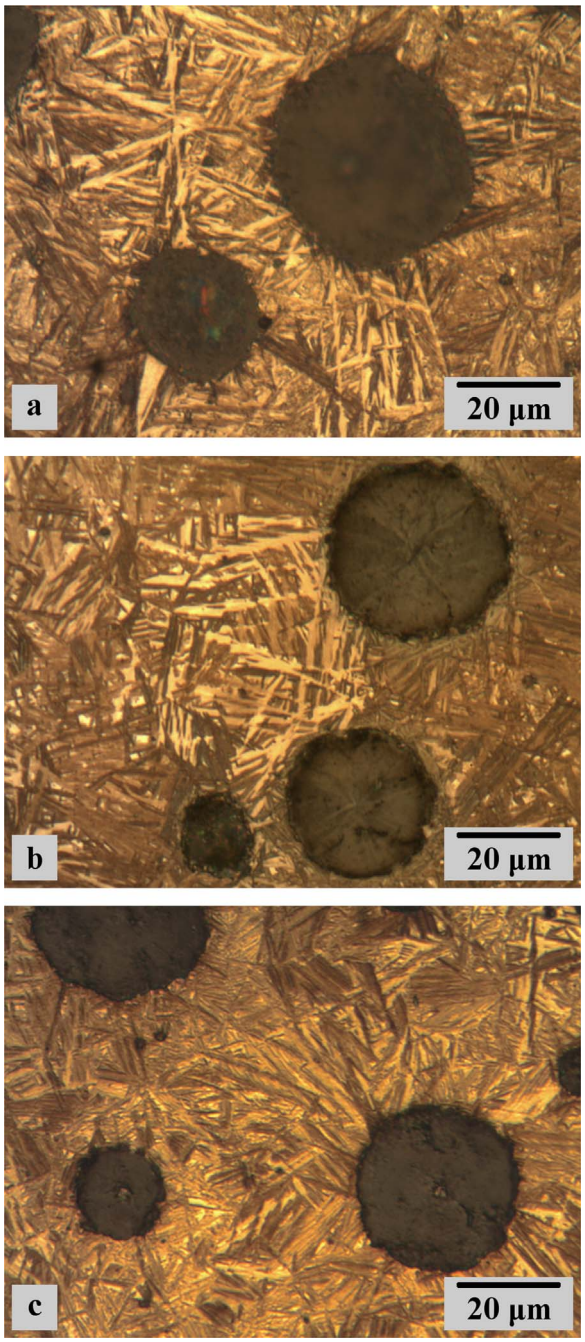

Fig. 3. Microstructure of ADI: (a) before deposition, (b) after deposition of Ti/TiN 0.7, (c) after deposition of Ti/TiN 1.5.

and coated samples was determined using a microhardness tester. Instrumented indentation was utilized to measure the hardness and elastic modulus of the coatings. Indentations were performed under applied loads of 5.8 mN and 15 mN for coating thicknesses of 0.7 µm and 1.5 µm, respectively. Coating adhesion was evaluated by the Rockwell-C adhesion test. A detailed description of the mentioned techniques was presented elsewhere [7]. Phase identification and residual stress measurements in the uncoated and coated samples were performed by x-ray diffraction (XRD). A Phillips XPERT-PRO diffractometer in the Bragg-Brentano (θ-θ) geometry was utilized at 40 kV and 40 mA, with Cu Kα radiation (λ=1.5418 Å). XRD patterns for phase identification were recorded in a 2θ range from 30° to 90° in steps of 0.02° and with a counting time of 1 s per step. Residual stress measurements were conducted using the $\sin^2\psi$ method, with the

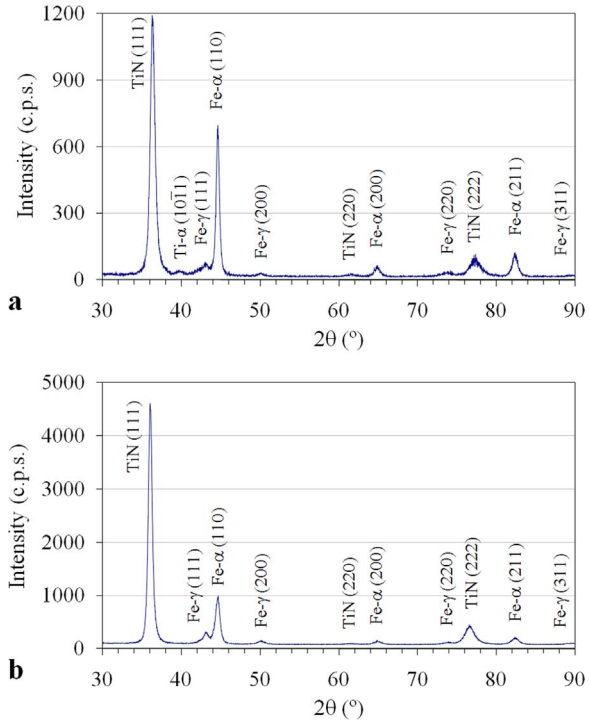

Fig. 4. DRX patterns of the coated samples: (a) ADI-Ti/TiN 0.7, (b) ADI-Ti/TiN 1.5.

assumption of a biaxial stress state. The optimal diffraction peak for measurements on the uncoated samples was Fe-α (222). The 2θ angle ranged from 134° to 140°, with a 2θ step of 0.05° and 5 s per step. The optimal diffraction peak for measurements on the coated samples was TiN (422). The 2θ angle ranged from 120° to 132° for TiN, with a 2θ step of 0.05° and 5 s per step. The x-ray elastic constants (XEC's) used to calculate stresses in uncoated and coated samples were extracted from bibliographic data [18–20]. Residual stress measurements in uncoated and coated samples were performed before the RCF tests in the perpendicular direction to the grinding scratches. Coating thickness was measured by means of the calotest method. Coating adhesion was also evaluated by scratch tests. A CSM Revetest scratch-tester equipped with a Rockwell indenter was employed. The coatings were tested using a progressive load ranging from 1 N to 100 N, a loading rate of 99 N/min, a speed of 5 mm/min and a scratch length of 5 mm. Critical loads were determined by post-tests optical microscopy. Three stages in the coating damage were considered, the first crack inside the scratch track (Lc1), the first delamination within the track (Lc2) and massive delamination (Lc3) [21].

2.4. Rolling contact fatigue tests

RCF tests were performed in a flat washer type testing rig using lubricated, pure rolling conditions. A detailed description of the RCF testing rig was presented in a previous work [7]. The maximum contact pressure (p_0) was set at 1400 MPa.

According to the Hamrock and Dowson equation [22], the RCF tests produced a minimum oil film thickness (h_0) close to 0.3 μm. Accordingly, the specific oil film thickness parameter (λ) of the uncoated and coated samples ranged from 0.79 to 1.47. Between these

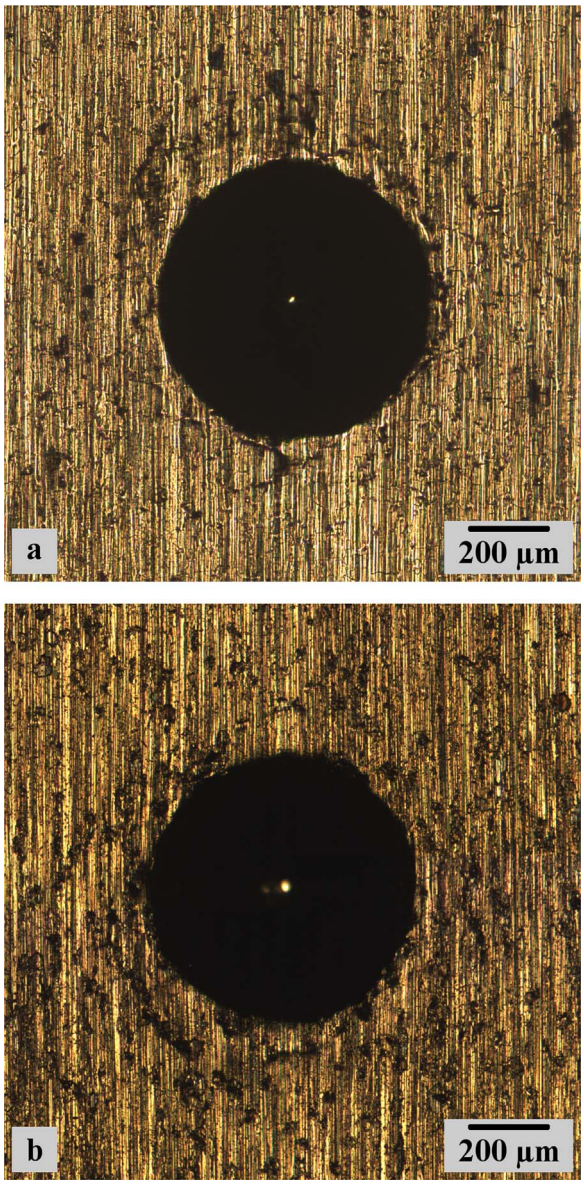

Fig. 5. Imprints on the Ti/TiN coated samples after Rockwell-C adhesion test: (a) ADI-Ti/TiN 0.7, (b) ADI-Ti/TiN 1.5.

Table 3
Scratch tests results.

Sample	Lc1 (N)	Lc2 (N)	Lc3 (N)
ADI-Ti/TiN 0.7	15.8 ± 2.4	22.6 ± 0.7	44.3 ± 2.3
ADI-Ti/TiN 1.5	16.2 ± 1.0	28.1 ± 1.3	48.6 ± 1.3

Table 2
Properties of the uncoated and coated samples.

Sample	Layer thickness		Ra (μm)	Surface hardness ($HK_{0.015}$)	Coating hardness (GPa)	Elastic modulus (GPa)	Residual stresses (GPa)
	Ti (μm)	TiN (μm)					
ADI	–	–	0.22 ± 0.03	720 ± 42	–	–	−0.41 ± 0.04
ADI-Ti/TiN 0.7	0.32 ± 0.02	0.78 ± 0.02	0.35 ± 0.04	1200 ± 95	21.4 ± 4.9	360 ± 52	−6.06 ± 0.13
ADI-Ti/TiN 1.5	0.31 ± 0.02	1.47 ± 0.03	0.38 ± 0.03	1580 ± 120	26.2 ± 6.9	359 ± 46	−6.86 ± 0.26

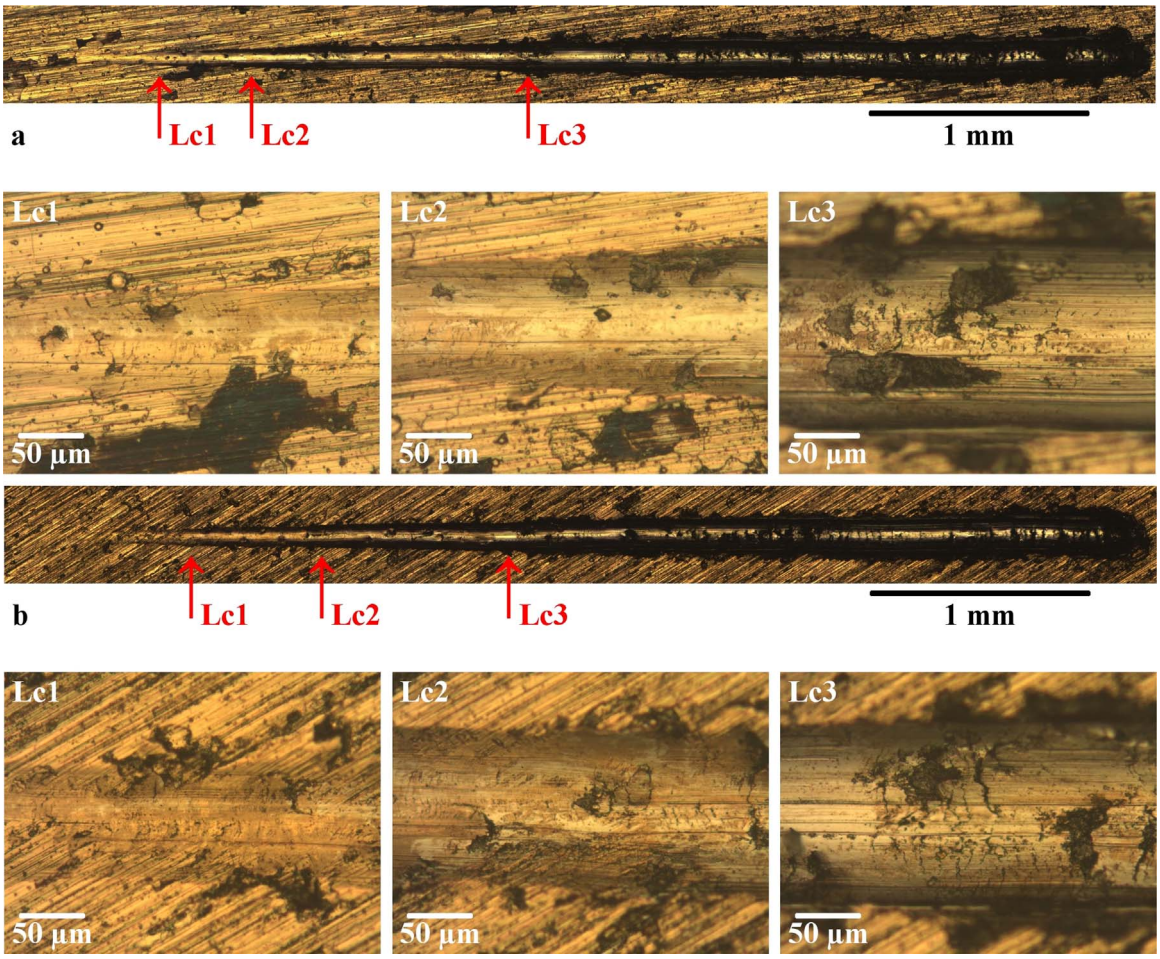

Fig. 6. Scratch tracks and coating damage features after the scratch tests: (a) ADI-Ti/TiN 0.7, (b) ADI-Ti/TiN 1.5.

limits, the contact bodies move so close to each other that there is considerable asperity interaction. It is well known that asperities act as stress raisers. Consequently, the nucleation of fatigue cracks will preferably take place on the samples surface.

Six RCF tests were carried out for each sample variant. In the case of the coated samples, the tests were performed in two stages. In the first stage, tests run until a macroscopic failure (coating delamination or substrate spalling) was formed on the samples surface. In the second stage, tests on delaminated samples were extended until substrate spalling. The rolling track of the tested samples was examined by SEM and EDS. Fatigue tests results were analyzed using the two-parameter Weibull distribution. Life data were fitted by rank regression, using the preferred X on Y ordering conversion. This method is the best practice for small data sets [23].

Life data were subjected to a statistical analysis in order to make inferences. Where high reliability is of prime importance, the main interest is in early failures [24]. For purposes of comparison, the 10% life (L_{10}) on the Weibull plot was used. The L_{10} life is the number of loading cycles within which 10% of the specimens can be expected to fail. This 10% life is equivalent to a 90% probability of survival. Two-sided 90% confidence intervals for each sample set were determined by Monte Carlo simulation with a pivotal statistic [23].

In addition, an alternative method developed to make inferences in multiple sets of samples was also employed [25]. The method consists of a test for the equality of shape parameters (or Weibull slopes) among the different groups of samples and, when a common shape parameter is found to be suitable, an interval and bias-corrected point estimation of any percentile. To test the homogeneity of shape parameters (β), the method defines the quantity ω given by the ratio of the largest estimated value of β to the smallest. Provided the population shape parameters are equal, ω is the ratio of two pivotal quantities and hence is itself pivotal [25]. The distribution of ω under the hypothesis that the different sets of samples have a common shape parameter depends on the number of sets (k), the set size (n) and the number of failures in each set (r) and can be estimated by Monte Carlo sampling. In practice, a difference in the population shape parameters among the different sets is manifested by a high value of ω. Therefore, an upper percentile value of the ω distribution is used as a critical value in the test for homogeneity of shape parameters.

3. Results and discussion

3.1. Ti layer characteristics

Table 1 lists the deposition time and thickness of the different Ti layers deposited on ADI.

Fig. 1 illustrates the diffraction patterns of the Ti coated samples. These patterns reveal not only the main diffraction peaks of the coating layers but also some peaks of the ferrite (Fe-α) and austenite (Fe-γ) phases, which belong to the substrates. All the films exhibited peaks related to the hexagonal close packed (hcp) Ti crystal structure, which is commonly denoted as α phase. On the other hand, the Ti layer with the lower film thickness exhibited an additional peak which could be associated with the face centered cubic (fcc) Ti phase [17]. According to previous studies [17,26], the presence of the fcc Ti phase was found to be dependent on the film thickness. The critical thickness above which no fcc Ti was observed was estimated in ~ 0.3 µm.

Fig. 2 compares the adhesion strength quality, determined by the

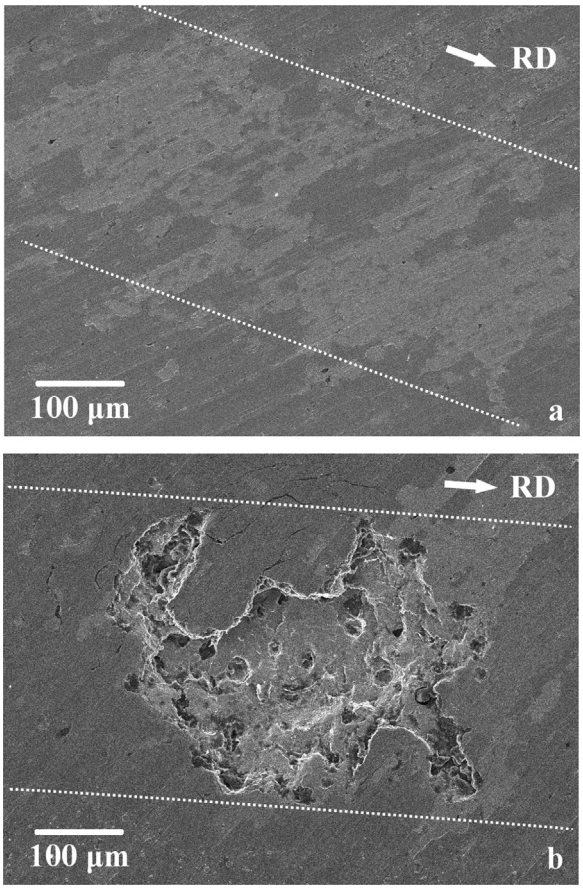

Fig. 7. Failure mechanisms observed in the Ti/TiN coated samples: (a) coating delamination, (b) substrate spalling.

Rockwell–C adhesion test, of the Ti layers to ADI substrates. The adhesion of the Ti layer with a film thickness of 0.3 µm can be classified as HF1 while the adhesion of the Ti layers with film thicknesses of 0.6 µm and 1.1 µm, as HF3 and HF 6, respectively. Although adhesion strength theoretically should increase as film thickness increases, there are reports that show an inverse behavior [11,27]. This might be caused by the increased difficulty in lattice match as the Ti layer thickness is increased. For that reason, a Ti layer thickness of 0.3 µm was selected for the Ti/TiN coated samples.

3.2. Substrates and Ti/TiN coatings characteristics

Fig. 3 compares the microstructure of ADI before and after coating deposition. It can be seen that the microstructure of the coated substrates is analogous to that of the uncoated substrate, both composed of acicular ferrite and retained austenite besides graphite nodules. Additionally, the amount of retained austenite and the surface hardness of the substrates were maintained between 17.5–18.7 vol% and 680–760 $HK_{0.015}$, respectively, before and after coating depositions. Therefore, it can be said that the coating processes are not harmful to the microstructure of ADI substrates.

Fig. 4 illustrates the diffraction patterns of the Ti/TiN coated samples. On all the samples, TiN layers grew with a preferred orientation of (111) planes parallel to their surface.

Table 2 lists the properties of the Ti/TiN coated samples, such as layer thickness, surface roughness, surface hardness, coating hardness, coating elastic modulus and residual stresses. The surface roughness, surface hardness and residual stress of the uncoated samples are also listed.

ADI substrates exhibit an average Ra value of 0.22 µm, an average surface hardness of 720 $HK_{0.015}$ and compressive residual stresses, with an average value of −0.41 GPa. According to a previous report [28], the residual stress values vary according to the orientation of the grinding scratches with respect to the measurement direction, being smaller in the perpendicular direction.

The average Ti and TiN layer thicknesses obtained were closer to their nominal values.

Regarding surface roughness, the coated samples present higher Ra than uncoated ADI but not a noticeable difference is observed between both coating thicknesses. The increase in Ra can be attributed to the presence of macroparticles (protrusions) in the coatings [29].

The average surface hardness varies from 1200 $HK_{0.015}$ in ADI-Ti/TiN 0.7 to 1580 $HK_{0.015}$ in ADI-Ti/TiN 1.5. This occurs because as coating thickness increases, the influence of the substrate hardness decreases. The coating hardness and elastic modulus does not vary significantly for both coating thicknesses analyzed.

The average residual stresses vary from −6.06 GPa in ADI-Ti/TiN 0.7 to −6.86 GPa in ADI-Ti/TiN 1.5, being compressive in all the cases. According to a previous report [28], the residual stress values of coated samples are independent of the measurement direction indicating a rotationally symmetric stress state.

The adhesion strength quality of the Ti/TiN coatings to the ADI substrates, as determined by the Rockwell–C adhesion test, can be classified as HF1. No delaminations were observed for any of the coating variants analyzed. Fig. 5 illustrates the imprints resulting from the Rockwell–C adhesion test.

According to previous reports [6,28,30], the introduction of a Ti interlayer between ADI substrates and TiN coatings does not produce significant changes in the characteristics of the coated samples.

The results of the scratch tests are presented in Table 3. It can be seen that the loads at the first crack inside the scratch track (Lc1) are very similar for both coating variants. On the other hand, the loads at the first delamination within the track (Lc2) and at massive delamination (Lc3) increase slightly as TiN coating thickness does. This behavior is consistent with previous studies [31,32] and can be associated with the fact that as coating thickness increases, an increased load is required to obtain the same degree of deformation. Fig. 6 shows the tracks resulting from the scratch tests together with the different coating damage stages.

3.3. Rolling contact fatigue behavior

3.3.1. First stage

In the first stage, as stated before, tests run until a macroscopic failure was formed on the surface of the coated samples. Two failure mechanisms were observed in the Ti/TiN coated samples, coating delamination and substrate spalling. Coating delamination turned out to be the most predominant failure mechanism and occurred at fewer loading cycles than substrate spalling. The behavior of the ADI-Ti/TiN 0.7 samples contrasts with the findings of a previous study, in which ADI samples coated with a 0.7 µm thick monolayer TiN film failed exclusively by substrate spalling [7]. The presence of the Ti interlayer may be responsible for this change. Fig. 7 shows the two failure mechanisms observed in the coated samples. The rolling direction (RD) is indicated on the micrographs.

Fig. 8 shows SEM micrographs taken inside the two types of failures encountered in the Ti/TiN coated samples as well as the corresponding EDS analysis. The micrograph of Fig. 8a shows the characteristic fracture surface of ADI inside a substrate spall. The corresponding EDS pattern (Fig. 8b) revealed the presence of Fe, C and Si, the main constituents of ADI. No Ti or N peaks were observed. On the other hand, the micrograph of Fig. 8c shows a delaminated area. Through this micrograph is impossible to determine whether the substrate was exposed or part of the Ti/TiN film remains adhered to the substrate. The corresponding EDS pattern (Fig. 8d) revealed the presence of Ti and N, indicating that the Ti interlayer and parts of the TiN layer remained adhered to the substrates inside the delaminated areas.

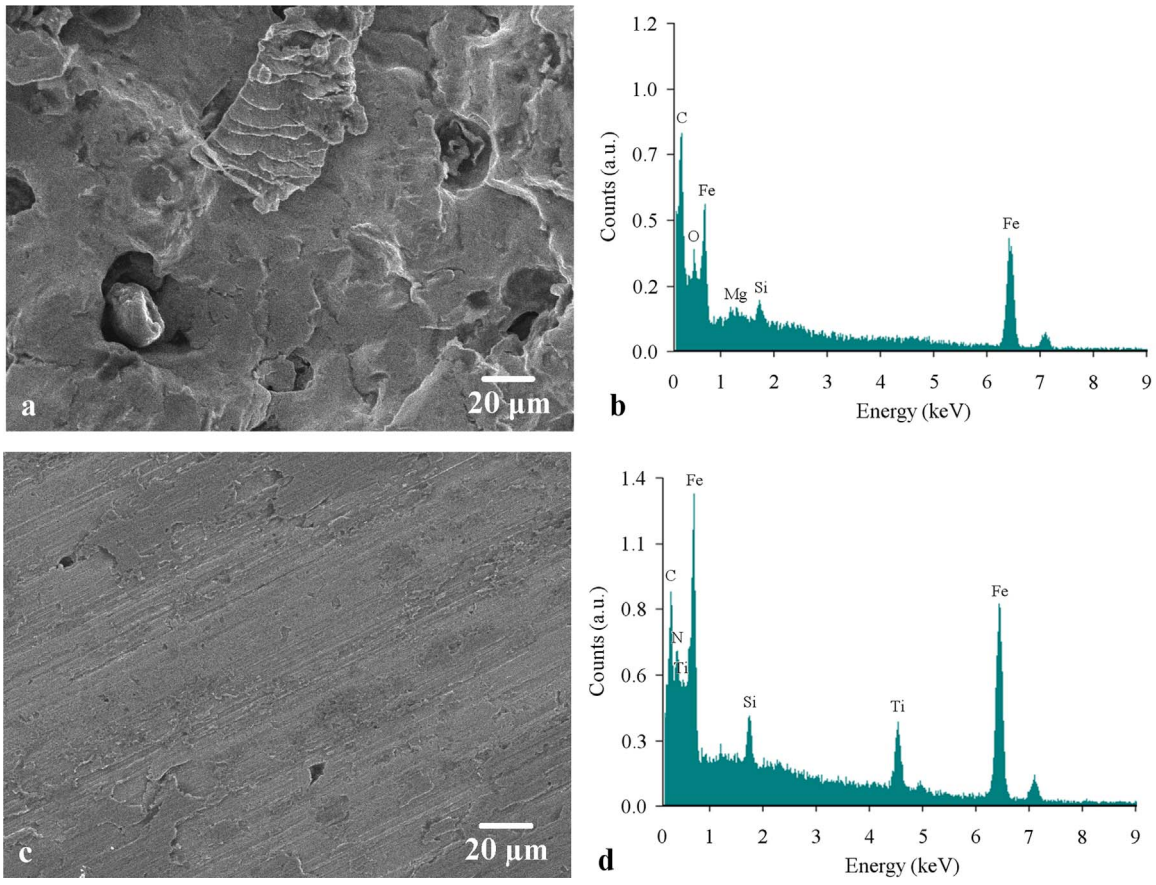

Fig. 8. SEM micrographs and EDS analysis of failures encountered in coated samples: (a) and (b) substrate spalling, (c) and (d) coating delamination.

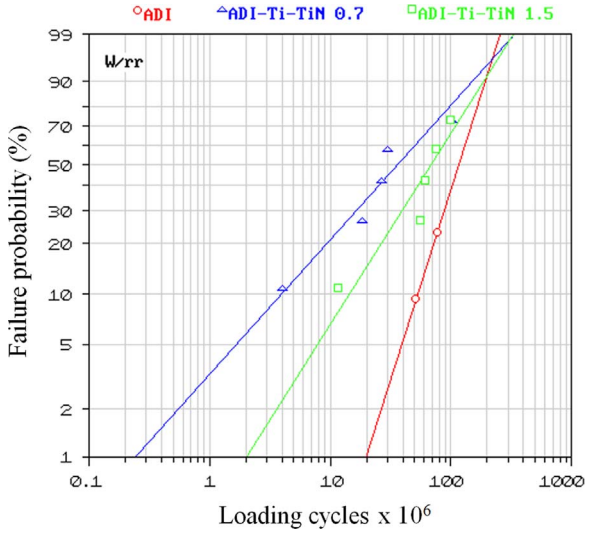

Fig. 9. Weibull plot for the uncoated and coated samples after first stage of tests.

Table 4
Estimates of the Weibull parameters for the uncoated and coated samples after first stage of tests.

Sample	β	η (cycles x10^6)	R^2
ADI	2.41	126	0.999
ADI-Ti/TiN 0.7	0.85	56	0.933
ADI-Ti/TiN 1.5	1.21	93	0.880

Table 5
Single and multiple set estimates of L_{10} for the uncoated and coated samples after first stage of tests and 90% confidence intervals.

Sample	Single set L_{10} (cycles x10^6)		Multiple set L_{10} (cycles x10^6)	
	Estimate	CI	Estimate	CI
ADI	49	0.96 – 82	42	2.9 – 90
ADI-Ti/TiN 0.7	3.9	0.12 – 16	13	2.8 – 24
ADI-Ti/TiN 1.5	14	1.2 – 38	17	3.7 – 31

Fig. 9 exhibits the Weibull plot of failure probability versus number of loading cycles for the Ti/TiN coated samples after the first stage. The curve of uncoated ADI is also shown for comparative purposes. The results of the Weibull analysis are summarized in Table 4, reflecting Weibull shape parameter (β), characteristic life (η, the estimated life for a failure probability of 63.2%) and coefficient of determination (R^2). According to the experimental data, the ratio of the largest estimated value of β to the smallest is 2.84. This value is lower than the 90th percentile of the ω distribution [25]. Thus, we consider that the different sets of samples have a common shape parameter. The common shape parameter was calculated using the free software Weibest.exe and yielded a value of 1.46. Table 5 lists the single and multiple set estimates of L_{10} for the uncoated and coated samples after first stage of tests. Two-sided 90% confidence intervals are also listed.

From Tables 4 and 5 it can be seen that η and the single and multiple set estimates of L_{10} for the coated samples are lower than those obtained for uncoated ADI. As stated before, coating delamination is the predominant failure mechanism in the coated samples. Consequently, the lower estimates of L_{10} for ADI-Ti/TiN 0.7 as compared to ADI-Ti/TiN 1.5 can be connected to its lower coating adhesion strength (see Table 3) [33]. However, the overlapping of the

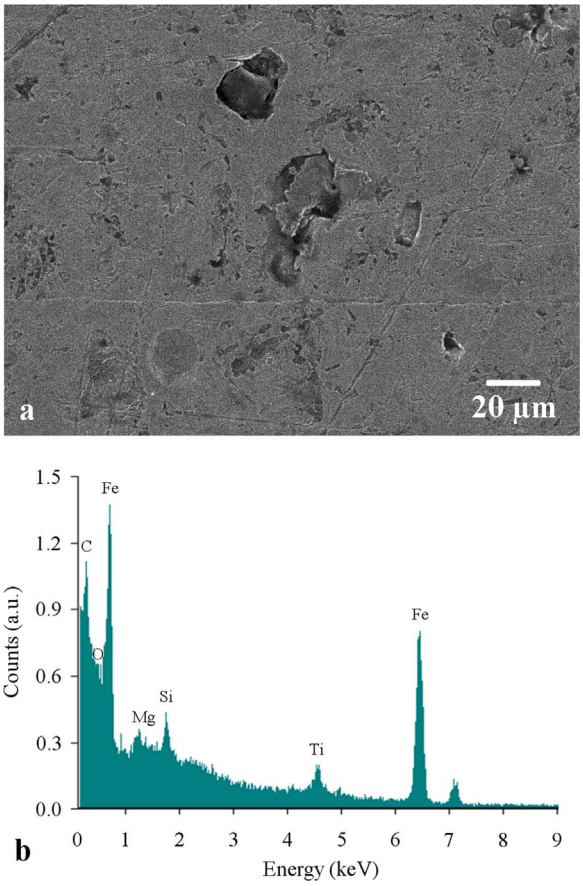

Fig. 10. Characteristics of the delaminated areas after final failure by substrate spalling: (a) SEM micrograph, (b) EDS analysis.

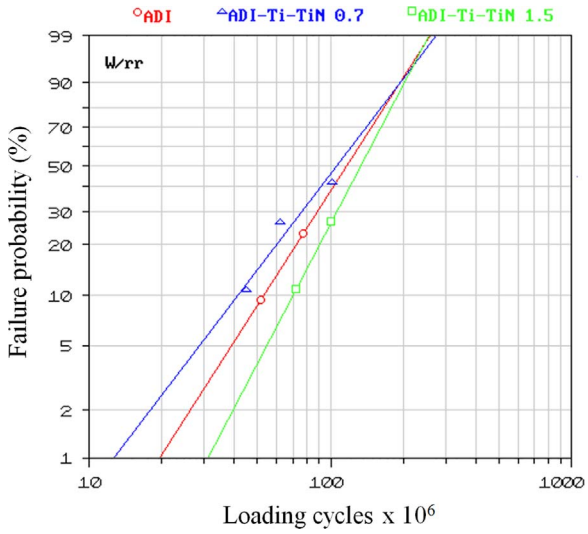

Fig. 11. Weibull plot for the uncoated and coated samples after second stage of tests.

Table 6
Estimates of the Weibull parameters for the uncoated and coated samples after second stage of tests.

Sample	β	η (cycles x10^6)	R^2
ADI	2.41	126	0.999
ADI-Ti/TiN 0.7	2.21	115	0.953
ADI-Ti/TiN 1.5	2.90	151	0.999

Table 7
Single and multiple set estimates of L10 for the uncoated and coated samples after second stage of tests and 90% confidence intervals.

Sample	Single set L_{10} (cycles x10^6)		Multiple set L_{10} (cycles x10^6)	
	Estimate	CI	Estimate	CI
ADI	49	0.96 – 82	66	19 – 94
ADI-Ti/TiN 0.7	42	6.7 – 68	55	16 – 80
ADI-Ti/TiN 1.5	69	3.0 – 107	69	20 – 99

confidence intervals does not allow to confirm the tendencies observed in the estimates of L_{10}.

3.3.2. Second stage

In the second stage, tests on samples that failed by coating delamination were extended until substrate spalling. As the RCF tests progressed, it was observed that the delaminated areas become enlarged within the rolling track, but inside these enlarged areas the Ti interlayer and parts of the TiN layer remained attached to the substrates until final failures by substrate spalling occurred. It is worth noting that substrate spalling preferably occurred in delaminated areas of the rolling track. Fig. 10a shows a SEM micrograph taken inside a delaminated area after substrate spalling occurred. The corresponding EDS pattern (Fig. 10b) revealed that the N signal is not detected and that the Ti peak diminished considerably.

Fig. 11 shows the Weibull plot for the Ti/TiN coated samples after the second stage. The curve of uncoated ADI is also shown for comparative purposes. The estimates of the Weibull parameters are summarized in Table 6. The ratio of the largest estimated value of β to the smallest is lower than the 90th percentile of the ω distribution [25]. Thus, we consider that the different sets have a common shape parameter which yielded a value of 3.14. The single and multiple set estimates of L_{10} for the uncoated and coated samples after second stage of tests are listed in Table 7. Two-sided 90% confidence intervals are also reported.

From Tables 6 and 7 it can be seen that η and the L_{10} estimates of the Ti/TiN coated samples are increased when only substrate spalling is considered as failure criterion. This behavior can be ascribed to the fact that the application of hard coatings tend to delay the substrate crack initiation process [34]. As mentioned before, substrate spalling preferably occurred in delaminated areas of the rolling track. Consequently, the higher estimates of L_{10} for ADI-Ti/TiN 1.5 as compared to ADI-Ti/TiN 0.7 can be related to its higher coating adhesion strength (see Table 3) which delays coating delamination and, consequently, the substrate crack initiation process. Again, the overlapping of the confidence intervals does not allow corroborating neither the influence of the TiN layer thickness on the behavior of the coated samples nor which set has the best behavior.

The high scattering in the estimates of L_{10} can be ascribed to the small number of samples used for each set in order to reduce the total testing time. The only way to reduce scattering in RCF is to increase the number of samples with the consequent increase of testing time. An alternative to reduce the testing time is to increase the maximum contact pressure used in the tests, but there is an upper limit since this pressure cannot produce material build up along the edges of the rolling track, which invalidates the tests.

Finally, if the results of this work are compared with previous findings [7], it can be seen that the introduction of a Ti interlayer does not significantly affect the RCF life of the TiN coated samples.

4. Conclusions

Ti/TiN coatings were applied on high strength ADI samples by CAD. The influence of the Ti interlayer and the TiN layer thickness on the characteristics and RCF behavior of the coated samples was

studied. Based on the results obtained, within the thickness range analyzed and the RCF test conditions used, the following conclusions can be drawn:

- Surface hardness, residual stresses and coating adhesion strength of the samples increase as TiN layer thickness increase while surface roughness, coating hardness and elastic modulus does not vary significantly with the TiN layer thickness.
- Regarding the RCF tests, two failure mechanisms were observed in the coated samples, coating delamination and substrate spalling. Coating delamination turned out to be the most predominant mechanism and occurred at fewer loading cycles than substrate spalling. The EDS analysis revealed that inside the delaminated areas the Ti interlayer remained adhered to the substrates. By conducting extended RCF tests on delaminated samples, it could be seen that the delaminated areas become enlarged until final failure by substrate spalling occurred. The EDS analysis revealed that inside these enlarged areas the Ti interlayer also remained adhered to the substrates. The Weibull analysis indicates that the RCF life of the coated samples seems to have a tendency to increase with the TiN layer thickness and, in the case of the thicker TiN layer, to exceed the life of uncoated ADI after the extended tests. However, due to the number of samples employed, the statistic analysis does not show significant differences in the RCF behavior of the uncoated and coated samples.

Acknowledgments

The financial support granted by the CONICET (Grant No. PIP 11220120100468CO), the ANPCYT (Grant No. PICT 2013–2630) the University of Buenos Aires (Grant No. PID 20020110100161) and the National University of Mar del Plata (Grant No. 15/G394) is gratefully acknowledged.

References

[1] R.C. Dommarco, P.C. Bastias, H.A. Dall'O, G.T. Hahn, C.A. Rubin, Rolling Contact Fatigue (RCF) resistance of Austempered Ductile Iron (ADI), Wear 221 (1998) 69–74.
[2] L. Magalhães, J. Seabra, C. Sá, Experimental observations of contact fatigue crack mechanisms for austempered ductile iron (ADI) discs, Wear 246 (2000) 134–148.
[3] R.C. Dommarco, J.D. Salvande, Contact fatigue resistance of austempered and partially chilled ductile irons, Wear 254 (2003) 230–236.
[4] R.C. Dommarco, A.J. Jaureguiberry, J.A. Sikora, Rolling contact fatigue resistance of ductile iron with different nodule counts and matrix microstructures, Wear 261 (2006) 172–179.
[5] C. Brunetti, M.V. Leite, G. Pintaude, Effect of specimen preparation on contact fatigue wear resistance of austempered ductile cast iron, Wear 263 (2007) 663–668.
[6] D.A. Colombo, M.D. Echeverría, S. Laino, R.C. Dommarco, J.M. Massone, Rolling contact fatigue resistance of PVD CrN and TiN coated austempered ductile iron, Wear 308 (2013) 35–45.
[7] D.A. Colombo, M.D. Echeverría, R.C. Dommarco, J.M. Massone, Influence of TiN coating thickness on the rolling contact fatigue resistance of austempered ductile iron, Wear 350–351 (2016) 82–88.
[8] D.S.R. Krishna, Y. Sun, Z. Chen, Magnetron sputtered TiO2 films on a stainless steel substrate: selective rutile phase formation and its tribological and anti-corrosion performance, Thin Solid Films 519 (2011) 4860–4864.
[9] Y.S. Hong, S.H. Kwon, T. Wang, D.-I. Kim, J. Choi, K.H. Kim, Effects of Cr interlayer on mechanical and tribological properties of Cr-Al-Si-N nanocomposite coating, Trans. Nonferrous Met. Soc. China 21 (Supplement 1) (2011) s62–s67.
[10] G.A. Fontalvo, R. Daniel, C. Mitterer, Interlayer thickness influence on the tribological response of bi-layer coatings, Tribol. Int. 43 (2010) 108–112.
[11] J. Tang, L. Feng, J.S. Zabinski, The effects of metal interlayer insertion on the friction, wear and adhesion of TiC coatings, Surf. Coat. Technol. 99 (1998) 242–247.
[12] B. Borawski, J.A. Todd, J. Singh, D.E. Wolfe, The influence of ductile interlayer material on the particle erosion resistance of multilayered TiN based coatings, Wear 271 (2011) 2890–2898.
[13] S.J. Bull, A.M. Jones, Multilayer coatings for improved performance, Surf. Coat. Technol. 78 (1996) 173–184.
[14] D.F. Diao, Y. Sawaki, H. Suzuki, Effect of interlayer on maximum contact stresses of hard coating under sliding contact, Surf. Coat. Technol. 86–87 (Part 2) (1996) 480–485.
[15] F.S. Shieu, L.H. Cheng, M.H. Shiao, S.H. Lin, Effects of Ti interlayer on the microstructure of ion-plated TiN coatings on AISI 304 stainless steel, Thin Solid Films 311 (1997) 138–145.
[16] D.A. Colombo, M.D. Echeverría, O.J. Moncada, J.M. Massone, PVD TiN and CrN coated austempered ductile iron: analysis of processing parameters influence on coating characteristics and substrate microstructure, ISIJ Int. 52 (2012) 121–126.
[17] M. Fazio, D. Vega, A. Kleiman, D. Colombo, L.M. Franco Arias, A. Márquez, Study of the structure of titanium thin films deposited with a vacuum arc as a function of the thickness, Thin Solid Films 593 (2015) 110–115.
[18] K.J. Martinschitz, R. Daniel, C. Mitterer, J. Keckes, Stress evolution in CrN/Cr coating systems during thermal straining, Thin Solid Films 516 (2008) 1972–1976.
[19] C.J. Smithells, E.A. Brandes, Metals Reference Book, 5th ed, Butterworth, London, UK, 1976, pp. 975–980.
[20] M. Zhang, J. He, Ab–initio calculation of elastic constants of TiN, Surf. Coat. Technol. 142–144 (2001) 125–131.
[21] Y.X. Ou, J. Lin, S. Tong, W.D. Sproul, M.K. Lei, Structure, adhesion and corrosion behavior of CrN/TiN superlattice coatings deposited by the combined deep oscillation magnetron sputtering and pulsed dc magnetron sputtering, Surf. Coat. Technol. 293 (2016) 21–27.
[22] B.J. Hamrock, D. Dowson, Isothermal Elastohydrodynamic Lubrication of Point Contacts: Part III - Fully Flooded Results, J. Lubr. Technol. 99 (1977) 264–275.
[23] R.B. Abernethy Fourth ed. The New Weibull Handbook. 2000. R.B. Abernethy, North Palm Beach, Florida, USA.
[24] B.L. Vlcek, E.V. Zaretsky, Rolling-Element Fatigue Testing and Data Analysis—A Tutorial, Tribol. Trans. 54 (2011) 523–541.
[25] J.I. McCool, Using the Weibull Distribution: Reliability, Modeling and Inference, Wiley, Hoboken, New Yersey, USA, 2012.
[26] J. Chakraborty, K. Kumar, R. Ranjan, S.G. Chowdhury, S.R. Singh, Thickness-dependent fcc–hcp phase transformation in polycrystalline titanium thin films, Acta Mater. 59 (2011) 2615–2623.
[27] A. Roshanghias, G. Khatibi, R. Pelzer, J. Steinbrenner, On the effects of thickness on adhesion of TiW diffusion barrier coatings in silicon integrated circuits, Surf. Coat. Technol. 259 (Part C) (2014) 386–392.
[28] D.A. Colombo, M.D. Echeverría, O.J. Moncada, J.M. Massone, Residual stress analysis in PVD coated austempered ductile iron, ISIJ Int. 53 (2013) 520–526.
[29] C.N. Tai, E.S. Koh, K. Akari, Macroparticles on TiN films prepared by the arc ion plating process, Surf. Coat. Technol. 43–44 (Part 1) (1990) 324–335.
[30] D.A. Colombo, M.D. Echeverría, O.J. Moncada, J.M. Massone, Characterisation of PVD–TiN coated austempered ductile iron: effects of nodule count and austempering temperature, ISIJ Int. 51 (2011) 448–455.
[31] P.A. Steinmann, Y. Tardy, H.E. Hintermann, Adhesion testing by the scratch test method: the influence of intrinsic and extrinsic parameters on the critical load, Thin Solid Films 154 (1987) 333–349.
[32] X. Nie, A. Leyland, H.W. Song, A.L. Yerokhin, S.J. Dowey, A. Matthews, Thickness effects on the mechanical properties of micro-arc discharge oxide coatings on aluminium alloys, Surf. Coat. Technol. 116–119 (1999) 1055–1060.
[33] Y.-H. Chen, I.A. Polonsky, Y.-W. Chung, L.M. Keer, Tribological properties and rolling-contact-fatigue lives of TiN/SiNx multilayer coatings, Surf. Coat. Technol. 154 (2002) 152–161.
[34] R. Ahmed, Rolling contact fatigue, in: W.T. Becker, R.J. Shipley (Eds.), ASM Handbook Volumen 11: failure analysis and prevention, ASM International, Materials Park, Ohio, USA, 2002, pp. 941–956.